Fakultät für Physik
Prof. Rupert Huber, Prof. Milena Grifoni

WS 15/16

Übungen zu Integrierter Kurs II - Festkörper und Statistische Physik

Blatt 7

Übungsleiter:

Dr. Andrea Donarini (3.1.24, phone 2040) (Theorie, Thu 8:30h - 12h, Phy 2.1.29)
Dr. Christoph Lange (2.0.07, phone 5704) (Experiment, Fr 12:30h - 14:00h, Phy 2.1.29)

Part I: Theory

7.1 Fermi pressure

Calculate the pressure of a non-relativistic Fermi gas $P(T, V, N)$ for $T \ll \epsilon_{\mathrm{F}}/k_{\mathrm{B}}$ where ϵ_{F} is the Fermi energy and k_{B} the Boltzmann constant. Discuss the limit $T \to 0$.
Hint: In order to determine the pressure it is useful to use the relation between energy and pressure of an ideal non-relativistic gas.

(1 Point)

7.2 Is the BEC a first order phase transition?

A transition is of first order if it is characterized by a finite latent heat $T\Delta S$. Is the Bose Einstein condensation a first order phase transition?
Hint: Use again the relation between pressure and energy as well as the fact that $PV = -J$ with J the grand canonical potential to determine the entropy per particle in a Bose system for $T \leq T_c$ as well as for $T \geq T_c$.

(3 Points)

7.3 Bose-Einstein condensation in a Gas of Sodium Atoms

The experimental proof of the BEC in alkali atoms gave the nobel prize to W. Ketterle, E. A. Cornell,and C. E. Wieman. Read the article below authored by W. Ketterle et al. and explain/comment the highlighted sentences (Sentences 1-4 in class). Moreover, reproduce the relation between the critical temperature and the density of particles for a BEC in an harmonic trap given in the third page of the paper (sentence 5).
To obtain the result, follow the following steps
Consider N spinless alkali atoms in a magnetic trap. The confinement potential can be simply approximated with the quadratic form

$$V_{\mathrm{ext}}(\mathbf{r}) = \frac{m}{2}\left(\omega_x^2 x^2 + \omega_y^2 y^2 + \omega_z^2 z^2\right),$$

where m is the mass of an alkali atom.

a) Write down the energy levels of the atoms in the trap.
(1 Point)

b) What is the critical chemical potential μ_c in the condensed state?
(1 Point)

c) Show that the difference between the total atom number N and that of the atoms in the ground state, N_0, is

$$N - N_0 = \zeta(3)\left(\frac{k_B T}{\hbar\omega_0}\right)^3,$$

with $\omega_0 = (\omega_x \omega_y \omega_z)^{1/3}$ and $\zeta(x)$ is the Riemann zeta function defined as

$$\zeta(x) = \frac{1}{\Gamma(x)} \int_0^\infty \frac{u^{x-1}}{e^u - 1} du = \sum_{n=1}^{\infty} \frac{1}{n^x}.$$

(2 Points)

d) Show that the critical temperature

$$k_B T_c = \hbar \omega_0 \left(\frac{N}{\zeta(3)} \right)^{1/3} = 0.94\, \hbar \omega_0 N^{1/3},$$

and therefore also obtain that the fraction of atoms in the ground state is

$$\frac{N_0}{N} = 1 - \left(\frac{T}{T_c} \right)^3.$$

(2 Points)

PHYSICAL REVIEW
LETTERS

VOLUME 75 27 NOVEMBER 1995 NUMBER 22

Bose-Einstein Condensation in a Gas of Sodium Atoms

K. B. Davis, M.-O. Mewes, M. R. Andrews, N. J. van Druten, D. S. Durfee, D. M. Kurn, and W. Ketterle
Department of Physics and Research Laboratory of Electronics, Massachusetts Institute of Technology, Cambridge, Massachusetts 02139
(Received 17 October 1995)

We have observed Bose-Einstein condensation of sodium atoms. The atoms were trapped in a novel trap that employed both magnetic and optical forces. Evaporative cooling increased the phase-space density by 6 orders of magnitude within seven seconds. Condensates contained up to 5×10^5 atoms at densities exceeding $10^{14}\,\mathrm{cm}^{-3}$. The striking signature of Bose condensation was the sudden appearance of a bimodal velocity distribution below the critical temperature of $\sim 2\ \mu$K. The distribution consisted of an isotropic thermal distribution and an elliptical core attributed to the expansion of a dense condensate.

PACS numbers: 03.75.Fi, 05.30.Jp, 32.80.Pj, 64.60.–i

Bose-Einstein condensation (BEC) is a ubiquitous phenomenon which plays significant roles in condensed matter, atomic, nuclear, and elementary particle physics, as well as in astrophysics [1]. Its most striking feature is a macroscopic population of the ground state of the system at finite temperature [2]. The study of BEC in weakly interacting systems holds the promise of revealing new macroscopic quantum phenomena that can be understood from first principles, and may also advance our understanding of superconductivity and superfluidity in more complex systems.

During the past decade, work towards BEC in weakly interacting systems has been carried forward with excitons in semiconductors and cold trapped atoms. BEC has been observed in excitonic systems, but a complete theoretical treatment is lacking [1,3]. The pioneering work towards BEC in atomic gases was performed with spin-polarized atomic hydrogen [4,5]. Following the development of evaporative cooling [6], the transition was approached within a factor of 3 in temperature [7]. Laser cooling provides an alternative approach towards very low temperatures, but has so far been limited to phase-space densities typically 10^5 times lower than required for BEC. The combination of laser cooling with evaporative cooling [8–10] was the prerequisite for obtaining BEC in alkali atoms. This year, within a few months, three independent and different approaches succeeded in creating BEC in rubidium [11], lithium [12], and, as reported in this paper, in sodium. Our results are distinguished by a production rate of Bose-condensed atoms which is 3 orders of magnitude larger than in the two previous experiments. Furthermore, we report a novel atom trap that offers a superior combination of tight confinement and capture volume and the attainment of unprecedented densities of cold atomic gases.

Evaporative cooling requires an atom trap which is tightly confining and stable. So far, magnetic traps and optical dipole traps have been used. Optical dipole traps provide tight confinement, but have only a very small trapping volume ($10^{-8}\,\mathrm{cm}^3$). The tightest confinement in a magnetic trap is achieved with a spherical quadrupole potential (linear confinement); however, atoms are lost from this trap due to nonadiabatic spin flips as the atoms pass near the center, where the field rapidly changes direction. This region constitutes a "hole" in the trap of micrometer dimension. The recently demonstrated "TOP" trap suppresses this trap loss, but at the cost of lower confinement [8].

We suppressed the trap loss by adding a repulsive potential around the zero of the magnetic field, literally "plugging" the hole. This was accomplished by tightly focusing an intense blue-detuned laser that generated a repulsive optical dipole force. The optical plug was created by an Ar^+-laser beam (514 nm) of 3.5 W focused

to a beam waist of 30 μm. This caused 7 MHz (350 μK) of light shift potential at the origin. Heating due to photon scattering was suppressed by using far-off-resonant light, and by the fact that the atoms are repelled from the region where the laser intensity is highest.

The experimental setup was similar to that described in our previous work [9]. Typically, within 2 s 10^9 atoms in the $F = 1$, $m_F = -1$ state were loaded into a magnetic trap with a field gradient of 130 G/cm; the peak density was $\sim 10^{11}$ cm^{-3}, the temperature ~ 200 μK, and the phase-space density 10^6 times lower than required for BEC. The lifetime of the trapped atoms was $\sim$ 30 s, probably limited by background gas scattering at a pressure of $\sim 1 \times 10^{-11}$ mbar.

The magnetically trapped atoms were further cooled by rf-induced evaporation [8,9,13]. rf-induced spin flips were used to selectively remove the higher-energy atoms from the trap resulting in a decrease in temperature for the remaining atoms. The total (dressed-atom) potential is a combination of the magnetic quadrupole trapping potential, the repulsive potential of the plug, and the effective energy shifts due to the rf. At the point where atoms are in resonance with the rf, the trapped state undergoes an avoided crossing with the untrapped states (corresponding to a spin flip), and the trapping potential bends over. As a result, the height of the potential barrier varies linearly with the rf frequency. The total potential is depicted in Fig. 1. Over 7 s, the rf frequency was swept from 30 MHz to the final value around 1 MHz, while the field gradient was first increased to 550 G/cm (to enhance the initial elastic-collision rate) and then lowered to 180 G/cm (to avoid the losses due to inelastic processes at the final high densities).

Temperature and total number of atoms were determined using absorption imaging. The atom cloud was imaged either while it was trapped or following a sudden switch-off of the trap and a delay time of 6 ms. Such time-of-flight images displayed the velocity distribution of the trapped cloud. For probing, the atoms were first pumped to the $F = 2$ state by switching on a 10 mW/cm^2 laser beam in resonance with the $F = 1 \rightarrow F = 2$ transition. 10 μs later the atoms were concurrently exposed to a 100 μs, 0.25 mW/cm^2 probe laser pulse in resonance with the $F = 2 \rightarrow F = 3$ transition, propagating along the trap's y direction. This probe laser beam was imaged onto a charge-coupled device sensor with a lens system having a resolution of 8 μm. Up to 100 photons per atom were absorbed without blurring the image due to heating.

At temperatures above 15 μK the observed trapped clouds were elliptical with an aspect ratio of 2:1 due to the symmetry of the quadrupole field. At the position of the optical plug they had a hole, which was used for fine alignment. A misalignment of the optical plug by ~ 20 μm resulted in increased trap loss and prevented us from cooling below 50 μK. This is evidence that the Majorana spin flips are localized in a very small region around the center of the trap. At temperatures below 15 μK, the cloud separated into two pockets at the two minima in the potential of Fig. 1. The bottom of the potential can be approximated as a three-dimensional anisotropic harmonic oscillator potential with frequencies $\omega_y^2 = \mu B'/(2mx_0)$, $\omega_z^2 = 3\omega_y^2$, $\omega_x^2 = \omega_y^2[(4x_0^2/w_0^2) - 1]$, where μ is the atom's magnetic moment, m the mass, B' the axial field gradient, w_0 the Gaussian beam waist parameter ($1/e^2$ radius) of the optical plug, and x_0 the distance of the potential minimum from the trap center. x_0 was directly measured to be 50 μm by imaging the trapped cloud, w_0 (30 μm) was determined from x_0, the laser power (3.5 W), and B' (180 G/cm). With these values the oscillation frequencies are 235, 410, and 745 Hz in the y, z, and x directions, respectively.

When the final rf frequency ν_{rf} was lowered below 0.7 MHz, a distinctive change in the symmetry of the velocity distribution was observed [Figs. 2(a) and 2(b)]. Above this frequency the distribution was perfectly spherical as expected for a thermal uncondensed cloud [14]. Below the critical frequency, the velocity distribution contained an elliptical core which increased in intensity when

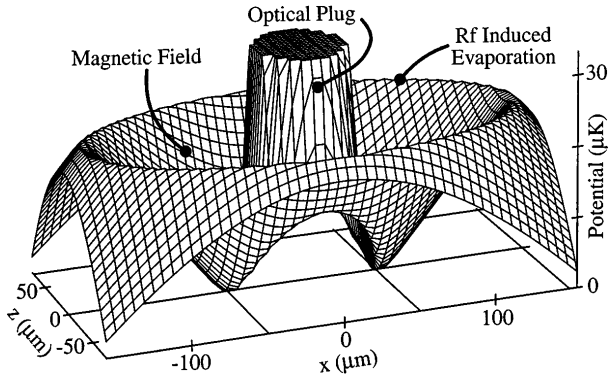

FIG. 1. Adiabatic potential due to the magnetic quadrupole field, the optical plug, and the rf. This cut of the three-dimensional potential is orthogonal to the propagation direction (y) of the blue-detuned laser. The symmetry axis of the quadrupole field is the z axis.

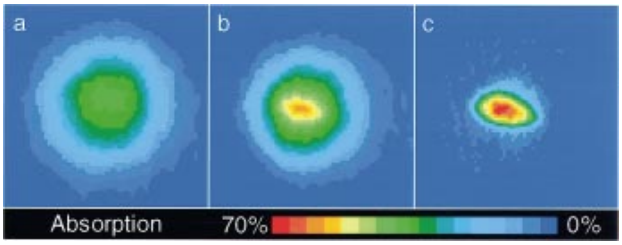

FIG. 2 (color). Two-dimensional probe absorption images, after 6 ms time of flight, showing evidence for BEC. (a) is the velocity distribution of a cloud cooled to just above the transition point, (b) just after the condensate appeared, and (c) after further evaporative cooling has left an almost pure condensate. (b) shows the difference between the isotropic thermal distribution and an elliptical core attributed to the expansion of a dense condensate. The width of the images is 870 μm. Gravitational acceleration during the probe delay displaces the cloud by only 0.2 mm along the z axis.

the rf was further swept down, whereas the spherical cloud became less intense. We interpret the elliptical cloud as due to the Bose condensate, and the spherical cloud as due to the normal fraction.

In the region just below the transition frequency one expects a bimodal velocity distribution: a broad distribution due to the normal gas and a narrow distribution due to the condensate. The cross sections of the time-of-flight images (Fig. 3) indeed show such bimodal distributions in this region. Figure 4 shows how suddenly the time-of-flight image changes below $\nu_{\rm rf} = 0.7$ MHz. The effective area of the observed cloud becomes very small [Fig. 4(a)], while the velocity distribution is no longer Gaussian [Fig. 4(b)] and requires different widths for the condensate and the normal fraction [Fig. 4(c)].

At the critical frequency, a temperature of (2.0 ± 0.5) μK was derived from the time-of-flight image. An independent, though less accurate estimate of the temperature T is obtained from the dynamics of evaporative cooling. Efficient evaporation leads to a temperature which is about 10 times smaller than the depth of the trapping potential [15]. Since the speed of evaporation depends exponentially on the ratio of potential depth to temperature, we expect this estimate of $T = 2$ μK to be accurate to within a factor of 2.

The critical number of atoms N_c to achieve BEC is determined by the condition that the number of atoms per cubic thermal de Broglie wavelength exceeds 2.612 at the bottom of the potential [2]. For a harmonic oscillator potential this is equivalent to $N_c = 1.202(k_B T)^3/\hbar^3\omega_x\omega_y\omega_z$ [16]. For our trap and 2.0 μK, $N_c = 2 \times (1.2 \times 10^6)$, where the factor of 2 accounts for the two separated clouds. The predicted value for N_c depends on the sixth power of the width of a time-of-flight image and is only accurate to within a factor of 3. We determined the number of atoms by integrating over the absorption image. At the transition point, the measured number of 7×10^5 agrees with the prediction for N_c. The critical peak density n_c at 2.0 μK is 1.5×10^{14} cm^{-3}. Such a high density appears to be out of reach for laser cooling, and demonstrates that evaporative cooling is a powerful technique to obtain not only ultralow temperatures, but also extremely high densities.

An ideal Bose condensate shows a macroscopic population of the ground state of the trapping potential. This picture is modified for a weakly interacting Bose gas. The mean-field interaction energy is given by $n\tilde{U}$, where n is the density and $\tilde{U}$ is proportional to the scattering length a: $\tilde{U} = 4\pi\hbar^2 a/m$ [2]. Using our recent experimental result $a = 4.9$ nm [9], $\tilde{U}/k_B = 1.3 \times 10^{-21}$ K cm^3. At the transition point, $n_c\tilde{U}/k_B T_c = 0.10$. Consequently, above the transition point, the kinetic energy dominates over the interaction energy, and the velocity

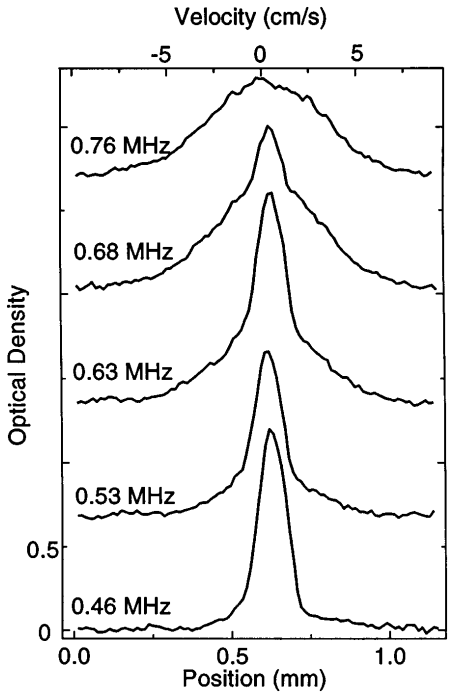

FIG. 3. Optical density as a function of position along the z axis for progressively lower values of the final rf frequency. These are vertical cuts through time-of-flight images like those in Fig. 2. For $\nu_{\rm rf} < 0.7$ MHz, they show the bimodal velocity distributions characteristic of the coexistence of a condensed and uncondensed fraction. The top four plots have been offset vertically for clarity.

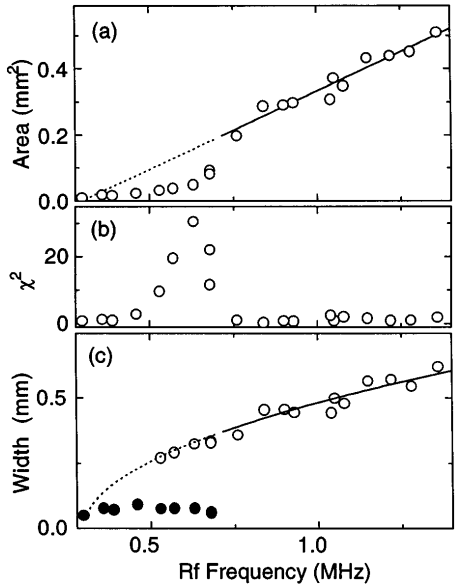

FIG. 4. Further evidence for a phase transition is provided by the sudden change of observed quantities as the final rf frequency $\nu_{\rm rf}$ is varied. (a) Area of the cloud in the time-of-flight image versus $\nu_{\rm rf}$. The area was obtained as the ratio of the integrated optical density and the peak optical density. The area changes suddenly at $\nu_{\rm rf} = 0.7$ MHz. Below the same frequency, the velocity distributions (Fig. 3) cannot be represented by a single Gaussian, as demonstrated by the χ^2 for a single Gaussian fit (b), and required different widths for the condensate (full circles) and noncondensate fraction (c). In (a) and (c) the lines reflect the behavior of a classical gas with a temperature proportional to the trap depth.

distribution after sudden switch-off of the trap is isotropic. For the condensate, however, the situation is reversed. As we will confirm below, the kinetic energy of the condensate is negligible compared to its interaction energy [17]. Furthermore, well below the transition point, the interaction with the noncondensate fraction can be neglected. In such a situation, the solution of the nonlinear Schrödinger equation reveals that the condensate density $n_0(\mathbf{r})$ is a mirror image of the trapping potential $V(\mathbf{r})$: $n_0(\mathbf{r}) = n_0(\mathbf{0}) - V(\mathbf{r})/\tilde{U}$, as long as this expression is positive, otherwise $n_0(\mathbf{r})$ vanishes (see, e.g., Refs. [5,18]). For a harmonic potential, one obtains the peak density $n_0(\mathbf{0})$ for N_0 atoms in the condensate $n_0(\mathbf{0}) = 0.118(N_0 m^3 \omega_x \omega_y \omega_z/\hbar^3 a^{3/2})^{2/5}$.

Typically, we could cool one-fourth of the atoms at the transition point into a pure condensate. For an observed $N_0 = 1.5 \times 10^5$, we expect the condensate to be 2 times more dense than the thermal cloud at the transition point, and about 6 times larger than the ground-state wave function. The kinetic energy within the condensate is $\sim \hbar^2/(2mR^2)$, where R is the size of the condensate [18], while the internal energy is $2n_0\tilde{U}/7$. Thus the kinetic energy of the condensed atoms is around 1 nK, much less than the zero-point energy of our trap (35 nK) and the calculated internal energy of 120 nK. This estimate is consistent with our initial assumption that the kinetic energy can be neglected compared to the interaction energy.

The internal energy is ~ 25 times smaller than the thermal energy $(3/2)k_B T_c$ at T_c. Consequently, the width of the time-of-flight image of the condensate is expected to be about 5 times smaller than at the transition point. This is close to the observed reduction in the width shown in Fig. 4(c). This agreement might be fortuitous because we have so far neglected the anisotropy of the expansion, but it indicates that we have observed the correct magnitude of changes which are predicted to occur at the BEC transition of a weakly interacting gas. In several cooling cycles, as many as 5×10^5 condensed atoms were observed; we estimate the number density in these condensates to be 4×10^{14} cm^{-3}.

A striking feature of the condensate is the nonisotropic velocity distribution [11,19]. This is caused by the "explosion" of the condensate due to repulsive forces which are proportional to the density gradient. The initial acceleration is therefore inversely proportional to the width of the condensate resulting in an aspect ratio of the velocity distribution, which is inverted compared to the spatial distribution. When we misaligned the optical plug vertically, the shape of the cloud changed from two vertical crescents to a single elongated horizontal crescent. The aspect ratio of the time-of-flight image of the condensate correspondingly changed from horizontal to vertical elongation. In contrast, just above the transition point, the velocity distribution was found to be spherical and insensitive to the alignment of the plug. However, we cannot account quantitatively for the observed distributions because we have two separated condensates which overlap in the time-of-flight images, and also because of some residual horizontal acceleration due to the switch-off of the trap, which is negligible for the thermal cloud, but not for the condensate [20].

The lifetime of the condensate was about 1 s. This lifetime is probably determined either by three-body recombination [21] or by the heating rate of 300 nK/s, which was observed for a thermal cloud just above T_c. This heating rate is much higher than the estimated 8 nK/s for the off-resonant scattering of green light and may be due to residual beam jitter of the optical plug.

In conclusion, we were able to Bose-condense 5×10^5 sodium atoms within a total loading and cooling cycle of 9 s. During evaporative cooling, the elastic collision rate increased from 30 Hz to 2 kHz resulting in a mean free path comparable to the dimensions of the sample. Such collisionally dense samples are the prerequisite for studying various transport processes in dense ultracold matter. Furthermore, we have reached densities in excess of 10^{14} cm^{-3}, which opens up new possibilities for studying decay processes like dipolar relaxation and three-body recombination, and for studying a weakly interacting Bose gas over a broad range of densities and therefore strengths of interaction.

We are grateful to E. Huang and C. Sestok for important experimental contributions, to M. Raizen for the loan of a beam pointing stabilizer, and to D. Kleppner for helpful discussions. We are particularly grateful to D. E. Pritchard, who not only contributed many seminal ideas to the field of cold atoms, but provided major inspiration and equipment to W. K. This work was supported by ONR, NSF, JSEP, and the Sloan Foundation. M.-O. M., K. B. D., and D. M. K. would like to acknowledge support from Studienstiftung des Deutschen Volkes, MIT Physics Department Lester Wolfe fellowship, and NSF Graduate Research Fellowship, respectively, and N. J. v. D. from "Nederlandse Organisatie voor Wetenschappelijk Onderzoek (NWO)" and NACEE (Fulbright fellowship).

[1] A. Griffin, D. W. Snoke, and S. Stringari, *Bose-Einstein Condensation* (Cambridge University Press, Cambridge, 1995).
[2] K. Huang, *Statistical Mechanics* (Wiley, New York, 1987), 2nd ed.
[3] J. L. Lin and J. P. Wolfe, Phys. Rev. Lett. **71**, 1222 (1993).
[4] I. F. Silvera and M. Reynolds, J. Low Temp. Phys. **87**, 343 (1992); J. T. M. Walraven and T. W. Hijmans, Physica (Amsterdam) **197B**, 417 (1994).
[5] T. Greytak, in Ref. [1], p. 131.
[6] N. Masuhara *et al.*, Phys. Rev. Lett. **61**, 935 (1988).
[7] J. Doyle *et al.*, Phys. Rev. Lett. **67**, 603 (1991).
[8] W. Petrich, M. H. Anderson, J. R. Ensher, and E. A. Cornell, Phys. Rev. Lett. **74**, 3352 (1995).

[9] K. B. Davis *et al.*, Phys. Rev. Lett. **74**, 5202 (1995).
[10] C. S. Adams *et al.*, Phys. Rev. Lett. **74**, 3577 (1995).
[11] M. H. Anderson *et al.*, Science **269**, 198 (1995).
[12] C. C. Bradley, C. A. Sackett, J. J. Tollett, and R. G. Hulet, Phys. Rev. Lett. **75**, 1687 (1995).
[13] D. E. Pritchard, K. Helmerson, and A. G. Martin, in *Atomic Physics 11*, edited by S. Haroche, J. C. Gay, and G. Grynberg (World Scientific, Singapore, 1989), p. 179.
[14] The measured $1/e$ decay time for the magnet current is 100 μs, shorter than the ω^{-1} of the fastest oscillation in the trap (210 μs). We therefore regard the switch-off as sudden. Any adiabatic cooling of the cloud during the switch-offtibs would result in a nonspherical velocity distribution due to the anisotropy of the potential.
[15] K. B. Davis, M.-O. Mewes, and W. Ketterle, Appl. Phys. B **60**, 155 (1995).
[16] V. Bagnato, D. E. Pritchard, and D. Kleppner, Phys. Rev. A **35**, 4354 (1987). This formula is derived assuming $k_B T_c \gg \hbar\omega_{x,y,z}$, which is the case in our experiment.
[17] Note that already for about 200 atoms in the ground state, the interaction energy in the center of the condensate equals the zero-point energy.
[18] G. Baym and C. Pethick (to be published).
[19] M. Holland and J. Cooper (to be published).
[20] These effects do not affect the vertical velocity distributions shown in Fig. 3.
[21] A. J. Moerdijk, H. M. J. M. Boesten, and B. J. Verhaar, Phys. Rev. A (to be published).

Part II: Experiment

7.1 Spezifische Wärmekapazität

Die spezifische Wärmekapazität bei konstantem Volumen, c_V, eines dreidimensionalen Kristalls ist gegeben durch

$$c_\mathrm{V} = \frac{C_\mathrm{V}}{V} = \frac{1}{V}\sum_{\vec{q},r}\frac{\partial}{\partial T}\frac{\hbar\omega_r(\vec{q})}{e^{\hbar\omega_r(\vec{q})/k_BT}-1}.$$

Hierbei ist r die Zahl der Phononenzweige und $k_\mathrm{B} = 1.3807 \cdot 10^{-23}\,\mathrm{J/K}$ die Boltzmann-Konstante.

(a) Berechnen Sie den Hochtemperaturlimes ($\hbar\omega_r(\vec{q}) \ll k_\mathrm{B}T$) von c_V für ein Gitter mit einer einatomigen Basis. (1 Punkt)

(b) Wie hängt $c_\mathrm{V}(T)$ in einem Isolator bei tiefen Temperaturen von T ab? Was bedeutet „tiefe Temperatur“ in diesem Zusammenhang? Was ist in einem Metall anders? Hinweis: Gehen Sie von einem großen Kristall aus, sodass Sie Summen im reziproken Raum durch Integrale ersetzen können. (1 Punkt)

(c) Was besagt die Debyesche Näherung? (1 Punkt)

(d) Wie hängt die phononische Zustandsdichte $D(\omega)$ im Debye-Modell bei kleinen Energien (im dreidimensionalen Fall) von ω ab? Begründen Sie Ihre Antwort. (1 Punkt)

(e) Schätzen Sie die Debye-Wellenzahl q_D, die Debye-Frequenz ω_D und die Debye-Temperatur Θ_D für Silber ab. Hinweis: Silber hat eine kubisch flächenzentrierte Kristallstruktur mit Gitterkonstante $a = 4.09\,\text{Å}$ und eine mittlere Schallgeschwindigkeit von 2600 m/s. (1 Punkt)

7.2 Spezifische Wärme eines eindimensionalen Gitters und eines Stapels aus zweidimensionalen Schichten

Analysieren Sie die spezifische Wärme eines eindimensionalen Gitters aus identischen Atomen.

(a) Zeigen Sie, dass in der Debye-Näherung die spezifische Wärme eines eindimensionalen Gitters aus identischen Atomen für tiefe Temperaturen ($T \ll \Theta_\mathrm{D}$) proportional zu T/Θ_D ist. Hierbei ist $\Theta_\mathrm{D} = \hbar\omega_\mathrm{D}/k_\mathrm{B} = \hbar\pi\nu_\mathrm{s}/k_\mathrm{B}a$ die für eine Dimension gültige Debye-Temperatur, k_B die Boltzmann-Konstante und a der Abstand der Gitteratome. (1 Punkt)

(b) Betrachten Sie einen dielektrischen Kristall, der aus einem Stapel von zweidimensionalen Atomschichten aufgebaut ist, wobei aneinandergrenzende Schichten nur schwach aneinander gebunden sein sollen. Wie sieht Ihrer Meinung nach der Ausdruck für die spezifische Wärme im Grenzfall sehr tiefer Temperaturen aus? (1 Punkt)

7.3 Inelastische Neutronenstreuung

Ein Strahl von Neutronen der Energie $E = 0.0540$ eV falle unter $\alpha = 90°$, $\beta = 90°$, $\gamma = 0°$ auf einen Bleikristall, wobei α, β, γ die Winkel mit der x-Achse, der y-Achse bzw. der z-Achse beschreiben. Die Bragg-Reflexion erfolgt unter der Richtung $\alpha' = 0°$, $\beta' = 90°$, $\gamma' = 90°$. Zur Ermittlung eines Punktes der Phononendispersionsrelation wird der unter $\alpha'' = 1.47°$, $\beta'' = 88.53°$, $\gamma'' = 90°$ gestreute Neutronenstrahl untersucht, für den die Energie $E'' = 0.0535$ eV gemessen wird. Berechnen Sie den Wellenzahlvektor $\vec{K}$, seinen Betrag und die Kreisfrequenz Ω der Phononen, die die zusätzliche Streuung hervorrufen. Blei hat ein fcc-Gitter mit der Gitterkonstanten $a = 0.494$ nm, der Kristall sei mit seinen Hauptachsen entlang des kartesischen Koordinatensystems ausgerichtet. (3 Punkte)

Hinweis: Die Impulserhaltung lautet in diesem Fall $\Delta\vec{k} = \pm\vec{K} + \vec{G}$, wobei $\Delta\vec{k}$ die Änderung des Wellenvektors der Neutronen ist, $\vec{K}$ der Wellenvektor des beteiligten Phonons und $\vec{G}$ ein reziproker Gittevektor. Konstruieren Sie sich die Basisvektoren des reziproken Gitters und finden Sie zunächst die reflektierende Netzebene bzw. $\vec{G}$, die für die elastische Neutronenbeugung verantwortlich ist. Sie können dann mit Hilfe der Impulserhaltung den Wellenvektor des Phonons berechnen.